Albumin-binding nanobody-antigen fusions enhance antigen presentation and improve vaccine responses through pharmacokinetic modulation

Hayden M. Pagendarm[1], Neil Chada[1], Alexander J. Kwiatkowski[2], Taylor Patino[2], Jonah Finkelstein[2], Christopher Lofts[3], Alexandra Lee[2], Jack Loken[2], Jody May[3], Blaise Kimmel[4], Karan Arora[2], John T. Wilson[1,2]

[1]Department of Biomedical Engineering, Vanderbilt University, Nashville, TN, USA; [2]Department of Chemical and Biomolecular Engineering, Vanderbilt University, Nashville, TN, USA; [3]Department of Chemistry, Vanderbilt University, Nashville, TN, USA; [4]Department of Chemical and Biomolecular Engineering, The Ohio State University, Columbus, OH, USA

VANDERBILT UNIVERSITY

IMMUNOENGINEERING LABORATORY

Role of Innate Immunity in Vaccination

- Antigen presenting cells (APCs) surveil their environment by sampling and presenting locally abundant antigens
- Innate immune system determines context of antigen presentation
  - Pattern recognition receptors (PRRs)
  - Pathogen associated molecular patterns (PAMPs)
- The context of antigen presentation determines the direction of the adaptive immune response

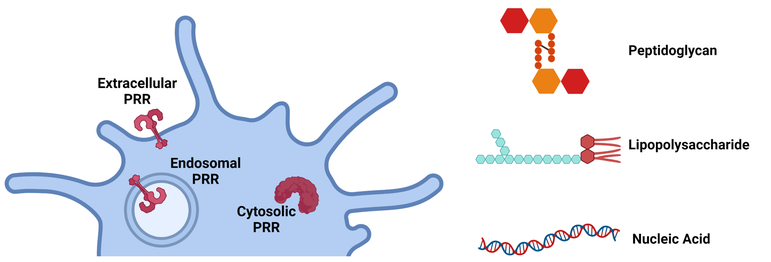

Figure 1. The recognition of pathogen associated molecular patterns (PAMPs) by pattern recognition receptors (PRRs) dictates how APCs interpret and present an antigen.

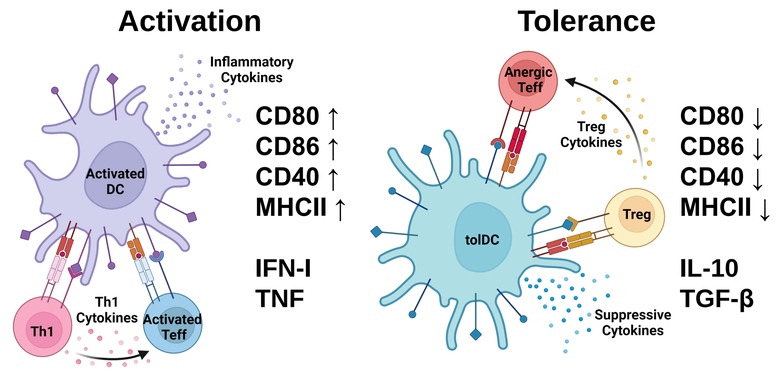

Figure 2. APCs educate and inform how T cells perceive and respond to an antigen through the expression of surface markers and the secretion of cytokines.

Albumin-Hitchhiking Enhances Lymphatic Drainage

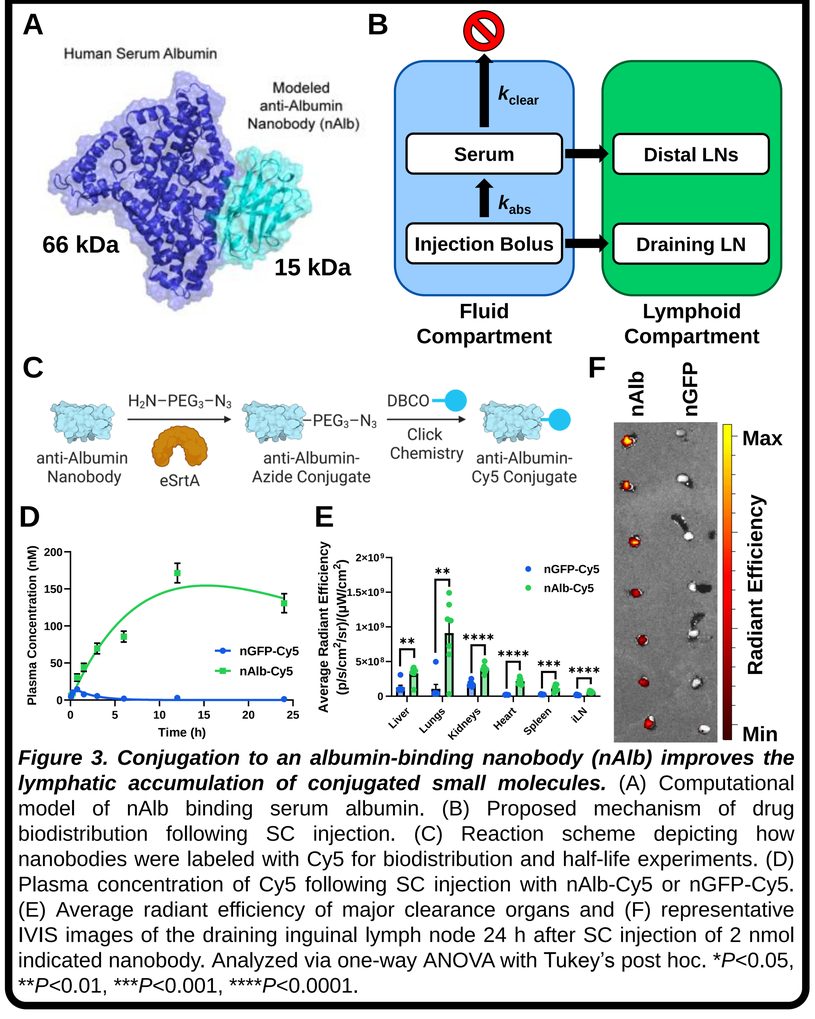

Figure 3. Conjugation to an albumin-binding nanobody (nAlb) improves the lymphatic accumulation of conjugated small molecules. (A) Computational model of nAlb binding serum albumin. (B) Proposed mechanism of drug biodistribution following SC injection. (C) Reaction scheme depicting how nanobodies were labeled with Cy5 for biodistribution and half-life experiments. (D) Plasma concentration of Cy5 following SC injection with nAlb-Cy5 or nGFP-Cy5. (E) Average radiant efficiency of major clearance organs and (F) representative IVIS images of the draining inguinal lymph node 24 h after SC injection of 2 nmol indicated nanobody. Analyzed via one-way ANOVA with Tukey's post hoc. *P<0.05, **P<0.01, ***P<0.001, ****P<0.0001.

nAlb Conjugation Increases Uptake by APCs

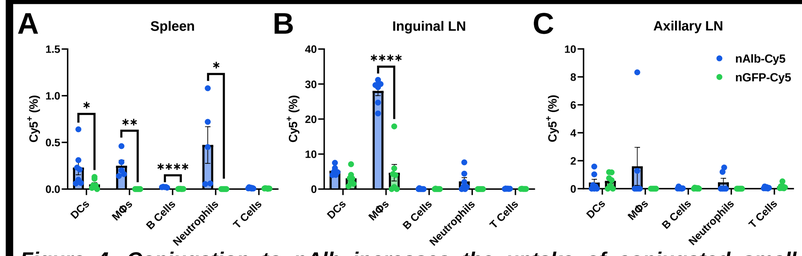

Figure 4. Conjugation to nAlb increases the uptake of conjugated small molecules by APCs across systemic lymphoid organs. Flow cytometric quantification of Cy5 uptake by major immune cell populations in the (A) spleen, (B) draining inguinal lymph node, and (C) irrelevant axillary lymph node 24 h after SC injection of 2 nmol Cy5. Analyzed via one-way ANOVA with Tukey's post hoc. *P<0.05, **P<0.01, ***P<0.001, ****P<0.0001.

Central Hypothesis

We can append peptide antigens and the appropriate immunomodulatory agents onto nAlb to develop a potent and tunable vaccine platform capable of driving both stimulatory and tolerogenic adaptive immune responses.

Prophylactic nAlb-MOG_{35-55} Treatment Inhibits EAE

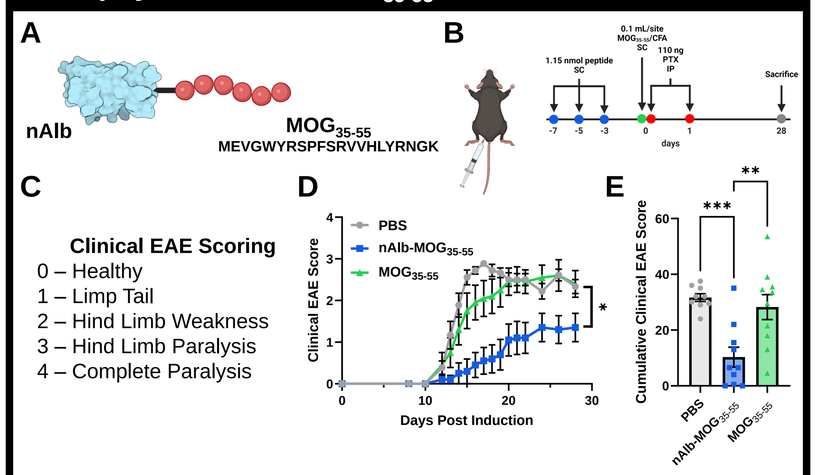

Figure 5. Prophylactic vaccination with an nAlb-MOG_{35-55} fusion inhibits disease progression in an experimental autoimmune encephalomyelitis (EAE) model of multiple sclerosis (MS). (A) Depiction of the nAlb-MOG_{35-55} fusion. (B) Experimental timeline of prophylactic treatments followed by disease induction using a commercially available kit. (C) Overview of the clinical EAE disease severity scoring criteria. (D) Average clinical EAE scores of each treatment group throughout the duration of the study. (E) Cumulative clinical EAE scores of each individual mouse throughout the duration of the study. Analyzed via one-way ANOVA with Tukey's post hoc. *P<0.05, **P<0.01, ***P<0.001, ****P<0.0001.

Rational Design of nAlb-Adjuvant Fusions

Motivation: Immunomodulatory adjuvants must also be conjugated to nAlb to achieve spatiotemporally coordinated delivery of antigen and adjuvant to APCs.

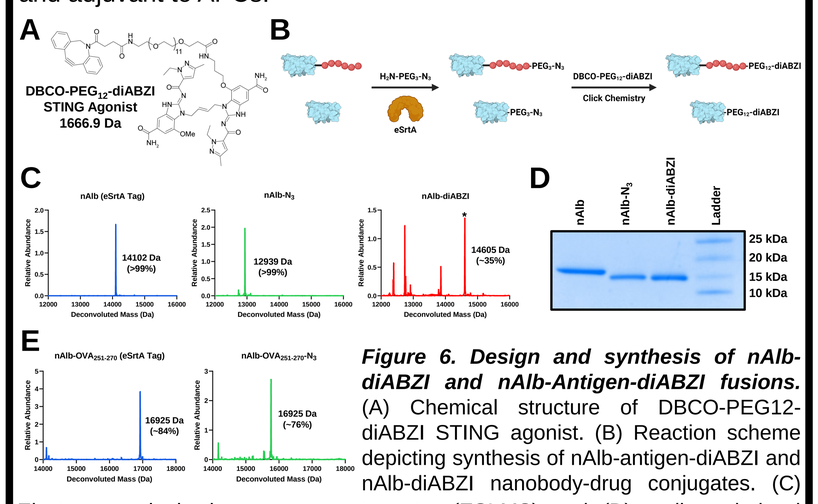

Figure 6. Design and synthesis of nAlb-diABZI and nAlb-Antigen-diABZI fusions. (A) Chemical structure of DBCO-PEG12-diABZI STING agonist. (B) Reaction scheme depicting synthesis of nAlb-antigen-diABZI and nAlb-diABZI nanobody-drug conjugates. (C) Electrospray ionization mass spectrometry (ESI-MS) and (D) sodium dodecyl sulfate polyacrylamide gel electrophoresis (SDS-PAGE) of nAlb, nAlb-N_3, and nAlb-diABZI constructs demonstrating nanobody-drug conjugate purity and molecular weight. (E) ESI-MS of nAlb-$OVA_{251-270}$ and nAlb-$OVA_{251-270}$-N_3 demonstrating nanobody-antigen fusion purity and molecular weight.

nAlb-Ag/nAlb-diABZI Vaccination

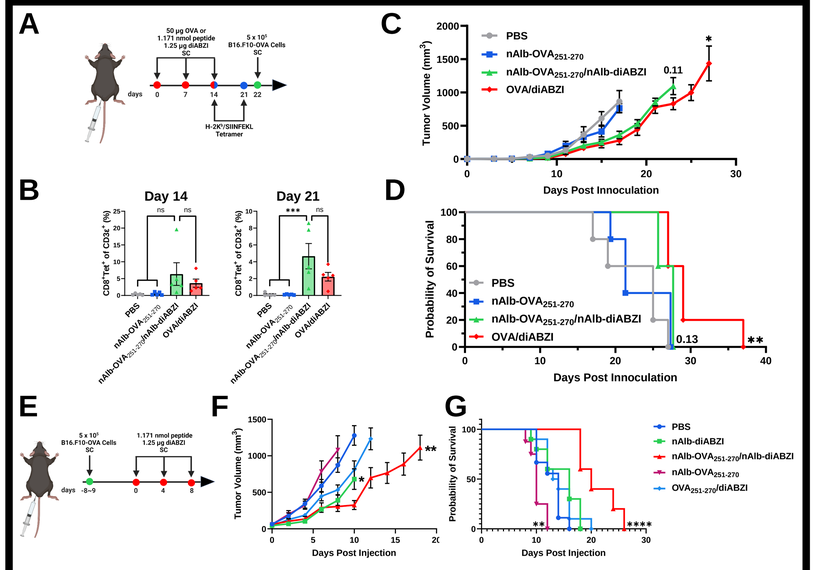

Figure 7. Vaccination with nAlb-$OVA_{251-270}$/nAlb-diABZI induces an antigen-specific $CD8^+$ T cell response with antitumoral effects. (A) Treatment timeline for tetramer analysis and prophylactic cancer vaccination with B16.F10-OVA challenge. (B) Percentage of $CD8^+Tet^+$ double-positive T cells in circulation following two or three doses of indicated vaccine constructs. (C) Tumor volumes following inoculation with $5x10^5$ B16.F10-OVA cells after prophylactic vaccination with indicated treatments. (D) Kaplan-Meier survival curves following treatment with indicated vaccine constructs. (E) Treatment timeline for therapeutic cancer vaccination model. (F) Tumor volumes following treatments with indicated vaccine constructs beginning when average volumes reached ~50-75 mm^3. (G) Kaplan-Meier survival curves following treatment with indicated vaccine constructs. Analyzed via one-way ANOVA with Tukey's post hoc or Mantel-Cox log-rank test. *P<0.05, **P<0.01, ***P<0.001, ****P<0.0001.

Fusion with nPD-L1 Boosts Vaccine Responses

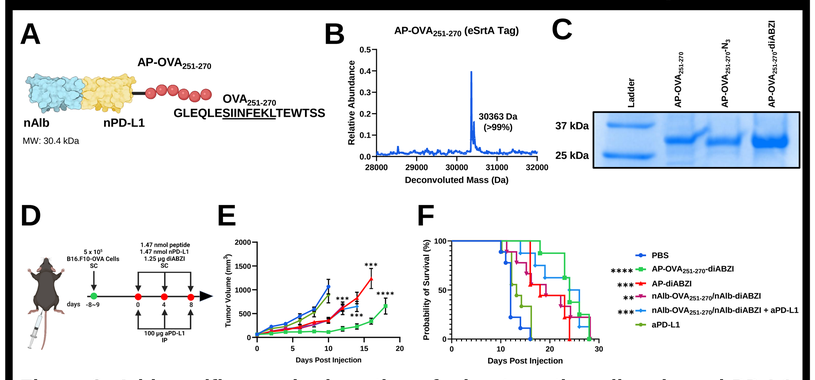

Figure 8. A bispecific nanobody-antigen fusion targeting albumin and PD-L1, conjugated to diABZI, improves antitumoral cancer vaccine responses compared to nAlb-$OVA_{251-270}$/nAlb-diABZI alone in a B16.F10-OVA model of melanoma. (A) Schematic of nAlb-nPD-L1-$OVA_{251-270}$ (AP-$OVA_{251-270}$) fusion. (B) Electrospray ionization mass spectrometry (ESI-MS) of AP-$OVA_{252-270}$ depicting mass and purity. (C) Sodium dodecyl sulfate polyacrylamide gel electrophoresis (SDS-PAGE) demonstrating mass of AP-$OVA_{252-270}$, AP-$OVA_{251-270}$-N_3, and AP-$OVA_{251-270}$-diABZI after each ligation step. (D) Treatment timeline of therapeutic B16.F10-OVA model. (E) Tumor volumes following treatment with indicated vaccine constructs beginning when the average tumor volume reached ~50-75 mm^3. Analyzed via one-way ANOVA with Tukey's post hoc. *P<0.05, **P<0.01, ***P<0.001, ****P<0.0001. (F) Kaplan-Meier survival curves following treatment with indicated vaccine constructs.

Acknowledgements

Funding:
- NIH R01 5R01CA266767-02
- NIH ITED T32 DK101003
- NSF GRFP 2022305770

Collaborators:
- Dr. Blaise Kimmel
- Wilson Lab

Figures made with Biorender.com